# A proposal of building new muon small wheels : the NSW project

Draft 0.00 30.06.2011

**Abstract**

*abstract*

## 1 Introduction [TK]

We propose to build a pair of new small wheel detector (NSW) to replace the existing ones during the second long shutdown[1] of the LHC during which the LHC will be upgraded to achieve its luminosity beyond the nominal design value and up to 2-3$\times 10^{34}$ cm$^{-2}$s$^{-1}$ in the following running period. The goal of NSW is to bring a significant enhancement of the muon performance in the endcap region, in particular of the level-1 muon trigger as well as the precision muon tracking, that would not be achieved by simple and thus lower cost modifications alone such as improvement of radiation shielding, addition of new detector layers or upgrade of electronics.

The muon small wheel is a part of the ATLAS muon spectrometer located in the endcap region in front of the endcap toroidal magnet. This is the innermost station of the three muon stations of the endcap. There are two identical sets of detectors in both sides of ATLAS. The small wheel consists of 4+4 layers of monitored drift tubes (MDT) for precision tracking in the bending direction ($R$ direction) and two layers of thin gap chambers (TGC) for azimuthal coordinates. These detectors cover the $\eta$ range of $1.3 < |\eta| < 2.0$. The inner part of the small wheel is covered by four layers of cathode readout chambers (CSC) because of its high rate capability. Each CSC layers determines both bending and azimuthal coordinates. The coverage of the CSC chambers is $2.0 < |\eta| < 2.7$.

Just to check if reference works [1]. Once more to see the order is OK [2].

## 2 Upgrade motivations [TK]

*Discussion of muon spectrometer performance at high luminosity - precision tracking and L1 trigger, and conclude that new detector and electronics are needed.*

*Point out serious (?) performance degradation in the small wheel region in both MDT and CSC, referring to the radiation background discussoin in Appendix. Performance of the present*

[1] Currently it is foreseen in 2018.

*detector should be evaluated for high lumi conditin, either using high lumi Monte Carlo or overlay of real events. CSC is 4 layers.*

*In the L1 discussion, emphasise the importance of maintaining low $p_T$ threshold. There are two issues. the high rate of fake triggers in the endcap region based mainly on the study using data. Then introduce basic idea of how this can be mitigated by integrating the small wheel in the L1 trigger. As the second point of trigger, discuss the pT resolution and possible improvement using the new small wheel. Physics requirement asks low pT threshold (20-40 GeV), L1 rate should be maintained at 100 kHz. Need sharpening pT threshold. Here introduce 1 mrad requirement.*

*Finally conclude that NSW should be built and replace the present ones as a phase-1 upgrade item in preparation to running with luminosity beyond the nominal luminosity.*

The Small Wheel (SW) is the first station ("Inner station") in the end-cap of the Muon spectrometer. Together with the Middle and Outer station it delivers the spatial coordinates for the momentum determination of charged tracks. Between the Small Wheel and the Middle station ("Big Wheel") a toroidal magnet is located with a bending power ranging from 3–7 T $\times$ m, depending on $\eta$, allowing a determination of the track momentum with high accuracy.

Designed to measure the momentum of a charged particle, the three stations of the end-cap have two distinct functions. They provide a fast, raw determination of the transverse momentum $p_T$, shortly after the passage of the particle, to be used by the Level-1 (L1) trigger. The L1 trigger logic has the task to identify events of physics interest, for which a high-$p_T$ muon is a crucial signature.

When a L1 trigger decision is broadcast to the ATLAS subsystems, the DAQ has to retain all relevant information for the corresponding beam crossing (BX). Because of technical limitations on data storage of the electronics, however, the L1-trigger must arrive at the subdetectors not later than 2,5 $\mu$s after particle passage (trigger "latency"), otherwise crucial information might be lost. This short L1 trigger latency of the present ATLAS readout system strongly limits the selectivity of the L1 decision, as only a fraction of the available tracking information can be used for a reduction of fake triggers, which are mainly due to low-$p_T$ tracks. One of the design aims for the ATLAS upgrade in phase II is an increase of the L1 trigger latency to 6,4 $\mu$s or even up to 10 $\mu$s. At this point more selective trigger strategies can be implemented, partly at the level of the frontend electronics, partly at the level of the Central Trigger Processor (CTP), where trigger information from different subdetectors can be combined.

The second important function of the three muon stations is the momentum measurement of the track with the highest available accuracy. This is achieved by combining high resolution drift tube chambers with a precise optical alignment system. Due to the alignment system the relative position of track hits in front and behind the bending magnet are precisely known, resulting in the required momentum resolution.

In the present Small Wheel Thin Gap Chambers (TGC) are used for the selection of high-$p_T$ tracks for the L1-trigger, while Monitored Drift Tube chambers (MDT) are used for the precision determination of the track coordinates.

The LHC upgrade in phase I and II will lead to an increase of the instantaneous luminosity

by a factor of 2 and 5, respectively. In the present SW, these high luminosities and the resulting background rates will lead to an unacceptable reduction in trigger and tracking efficiency.

The main shortcoming of the present L1-trigger in the end-cap is caused by the fact that a majority of tracks crossing the SW do not originate from the primary vertex and should therefore not be considered candidates for a high-$p_T$ muon by the triggering system. The present trigger, however, can not determine the slope of the candidate track in the r-z plane and for this reason is unable to discard tracks not coming from the primary vertex. The trigger chambers of the New Small Wheel (NSW) will have to be able to determine the slope of the track with an accuracy of $< 1$ mrad in the r-z plane (bending plane). The slope of the track must also be determined in the $\phi$ direction, though with less accuracy, to further reduce the number of trigger candidates which do not come from the interaction point.

| Chamber Type | location in r | tube length | expected hit rate | rate per tube | occup-ancy | effi-ciency |
|---|---|---|---|---|---|---|
| | *cm* | *cm* | *hits/cm²* | *kHz* | *%* | *%* |
| EIL0 | 150 cm | 75 cm ?? | 2000 | 2 kHz | 85 % | xx |
| EIL1 | 262 cm | 152 cm | 300 | 0,3 kHz | 92 % | xx |
| EIL2 | 373 cm | 206 cm | 100 | 0,1 kHz | 98 % | xx |

Table 1: Expected hit rates and efficiencies for 15 mm tubes in the NSW. (Numbers are mostly dummies and have to be worked out later!

The limitations of the MDT precision chambers at high luminosity are mainly caused by isolated hits in the tubes ("fake hits"), caused by neutron and gamma conversions in nearby support structures, tube walls, chamber gas and tungsten wires. The presently used 30 mm diameter tubes ("Large tubes") start to lose efficiency if hit rates go beyond about 300 kHz per tube. While the length of the tubes in the trapezoidal geometry of the SW decreases proportional to distance from the beam line (r), the background rates increase considerably faster than with 1/r. The highest hit rates per tube thus occur at the inner tip of the EIS and EIL chambers. The observed losses of efficiency and spatial resolution in the drift tubes are partly due to positive ions, slowly drifting in the tube gas, distorting electric field and drift velocity, partly due to a reduction of the electric field close to the wire, reducing gas amplification and signal height [9]. Bandwidth limitations of the present readout electronics also contribute to the loss of efficiency (see section 5.4 below). Replacing the present MDTs by a chamber type with higher rate capabilities and improving the readout electronics correspondingly is therefore a central aim for the Small Wheel upgrade towards higher luminosities, as expected from the SLHC.

Table 1 gives background rates, occupancies and hit efficiencies for MDT tubes at different radii in the SW, based on simulation work in Ref. [3]. Results form LHC running at luminosities up to $5 \times 10^{32}$ seem to indicate rates which are about a factor 3–4 above the simulated ones for the innermost chambers EIS1 and EIL1 of the SW.

# 5 Detector concept 1 : MDT + TGC (working title)

*Introduction to this concept: This section should describe the technology concept, details up to the level of a single chamber should be given in the appropriate appendix.*

## 5.1 Introduction

Tu cure the shortcomings of the existing system, a new concept is proposed for the Inner station, the New Small Wheel (NSW). For the trigger chambers we propose to maintain the basic operating concept of TGC chambers, complementing them with a new, high-performance readout system. The pulseheight distribution of signals induced into the strips of the TGC cathodes (measuring $\eta$) are convoluted to give the precision coordinate with an accuracy of $<$100 $\mu m$. With modern, radiation-tolerant FPGAs the location of the hits can be determined fast enough for the L1 trigger. In the proposed detector layout, a package of 4 TGC chambers is placed in front and behind the MDT chambers, each. A TGC package will contain 4 wire layers (wires running radially, perpendicular to the strips), 4 cathode layers for centroide finding and another 4 cathode layers segmented into pads for fast selection of a Region of Interest (RoI). In the offline analysis the pads will be an important tool for resolving ambiguities in the x-y pairing of coordinates, when more than one track is present in a chamber. With a distance of about 300 mm between the TGC packages in front and behind the MDT, an angular resolution of $< 0,3$ mrad can be achieved. Only tracks pointing to the interaction point will be considered as high-$p_T$ candidates for the L1 trigger. A detailed presentation of the method is given in section 5.4.

The problem of high tube occupancies of the MDT is solved by using a newly developed type of MDT drift tubes, the tube diameter being reduced from 30 mm to 15 mm. While the tube area exposed to background radiation is thus reduced by a factor of two, the maximum drift time is reduced by a factor of 3,5 (750 ns to 200 ns), the combined effect giving a reduction of hit rates by a factor of 7. The mechanical structure and the alignment system will be as similar as possible to the ones in the present SW architecture. Like in the case of the TGCs, faster readout electronics has to be installed, see section 5.5.

Both new chamber systems, the TGCs and the MDTs, can be operated with the same chamber gas as in the present system. Power requirements for the electronics of both systems will be higher due to higher channel count. Whether this requires active cooling, as is now used for the electronics of the CSC chambers in the region $\eta > 2$ is under study. Aim is to have services arranged in such a way as to be able to use the existing service infrastructure like e.g. the cable Schlepps.

## 5.2 Detector technology and layout

*Description of detector concept (a detailed description of the working principle of each detector should be given as an appendix).*
*If more than 1 technology is used motivate the decision and detail how they work together (e.g.*

*can services be shared, is the information of the trigger chambers used in the precision chambers, how are combined chambers assembled etc.)*

*List of all operating parameters*
*Detailed layout: acceptance, description of chamber overlap and dead areas, drawings*
*Tables with chambers sizes, number of channels*
*Internal alignment scheme (the overall common endcap alignment scheme is described in the previous chapter)*
*Calculations about mechanical stability and expected deformations due to gravity, temperature changes, (magnetic field) etc.*
*Requirements for mount points*
*Details of service points and other positions where access is needed*
*Concept for chamber replacement (what needs to be dismounted etc.)*

### 5.2.1 Detector technology of the TGC chambers

Text about TGCs.

### 5.2.2 Detector technology of the MDT chambers

The outer region of the ATLAS detector, where the muon chambers are located, receives high rates of low-energy neutrons, mainly due to shower leakage from calorimeters and shielding structures in the high-$\eta$ region. At the nominal luminosity, gammas from neutron capture and related conversion electrons are expected to generate hit rates in the range 50–300 kHz in each MDT tube. A conversion electron may create an inefficiency if the signal arrives *before* the muon signal. The muon detection efficiency thus becomes $\exp(-\tau \times f) \approx 1-\tau \times f$, where $\tau$ is the average drift time in the MDT tubes and f the hit rate due to gamma conversions.

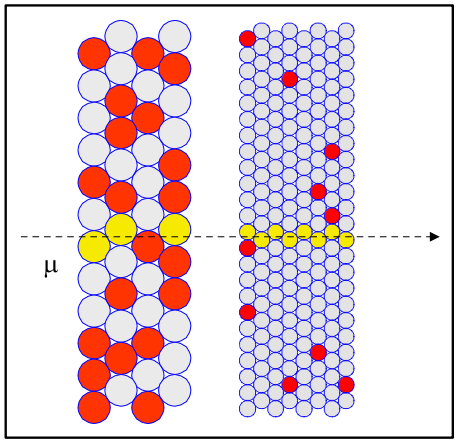


Figure 1: The tracking quality in 30 mm and 15 mm drift tubes in a region of high n/$\gamma$ background. The occupancies from background hits (red dots) are 50% in the 30 mm tubes but only 7% in the 15 mm tubes due to shorter drift time and smaller area.

At high rates of n/$\gamma$ background, the efficiency may be further reduced by a decrease of the gas amplification due to space charge from slowly drifting positive ions in the tubes, while the *fluctuations* of the space charge tend to degrade the spatial resolution by up to about 20 % at the highest rates.

The effects of gamma conversions in the MDT tubes have been studied in detail using a muon beam in the presence of intense $\gamma$-irradiation of up to 500 Hz/cm$^2$ (i.e. ~300 kHz/tube), as delivered by the Gamma Irradiation Facility at CERN (GIF) [9]. While the $\gamma$-rates at the GIF correspond to only about 30 % of the background levels expected for the hottest regions at the SLHC, the results of these measurements already allow to define the baseline of a chamber design with much improved tracking capability: MDT drift tubes with only half the tube diameter offer a reduction of the drift time by a factor 3.5, due to the non-linear relation between track distance from the central wire and drift time (r-t relation) and in addition by a factor 2 from the exposed area, thus yielding a factor 7 in the reduction of the hit rate due to n/$\gamma$ background. Moreover, up to two times more tube layers can in principle be accommodated in the available space, leading to improved track finding efficiency and position resolution (see Fig. 5.2.2).

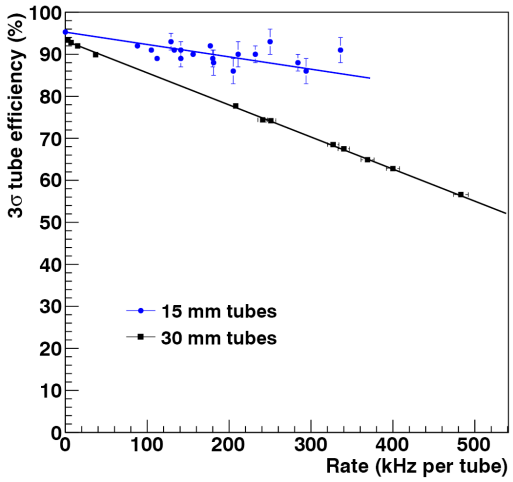


Figure 2: Efficiency vs. hit rate per tube for 30 mm and 15 mm drift tubes.

The reduction of the tube diameter of the MDT tubes allows to maintain the main advantages of the drift tube concept:

(a) independence of the position resolution from the angle of incidence onto the chamber plane (contrary to drift chambers with rectangular drift geometry)

(b) operational independance of each tube, where the malfunction of a tube can only generate a negligible inefficiency

(c) modularity of chamber construction.

To verify the performance of 15 mm ("small") tubes, a number of tests was executed, using cosmic muon tracks. A pair of 30 mm ("large") drift tube chambers was used as reference, defining the position of the muon track, while a layer of small tubes was the device under test.

Tubes along the track are called 'efficient' when the hit is detected inside a $3\sigma$ road, as defined by the reference tubes.

This measurement was done in the presence of adjustable levels of gamma background due to the GIF facility at CERN [10]. Fig. 2 shows the efficiency of small and large tubes vs. hit rate from gamma conversions. As expected, small tubes provide a much better performance at high background rates. The efficiency at rate zero deviates from 100 % due to tracks passing across or close to the tube walls and due to $\delta$-electrons shifting the hit position outside the $3\sigma$ acceptance road. The average position resolution in the small tubes was about 120 $\mu$m. Due to the short drift compared to large tubes, this value showed little dependence on the background rate.

## 5.3 Performance

*Summary of chamber performance, details in appendix of technology.*

*Spatial and angular resolution as functions of rate and angle of incidence*
*Time resolution*
*Efficiency (single measurement and segment)*
*Double track resolution*
*Rejection of fake and background tracks*

## 5.4 L1 trigger and electronics

*How the L1 signal are produced, starting from the detector signal till the formation of SL input.*
*Latency (calculation, measurement with demonstrator)*
*Compatibility with Phase II upgrade RR to supply text !!!*

## 5.5 Readout electronics and integration in DAQ

*Detailed description of electronics chain.– Integration to DAQ (Mention the GBT?).– Readout related parameters, e.g. bandwidth requirements, number and granularity of read-out links.– Compatibility with Phase II upgrade.*

The readout of the Small MDT tubes will follow the proven architecture of the present MDT system. A number of additions and modifications, however, will be necessary in order to adapt the rate capability of the readout chain to the requirements of the SLHC. For the mechanical integration of the readout electronics with the Small tube chambers, the layout of the electronics will have to be adapted to the 4 times higher tube density at the ends of the Small tube chambers. Finally, the radiation tolerance of all components will have to comply with the high radiation levels, in particular at the inner border of the Small Wheel.

### 5.5.1 Architecture of the present MDT readout

In the present readout scheme tube signals are routed via a PCB ("hedgehog card") to a piggy-back card ("mezzanine card"), containing an Amplifier and Shaper, followed by a Discriminator with adjustable threshold, all three functions being integrated in a radiation tolerant ASIC (ASD). The discriminator outputs, in turn, are routed to a TDC, where each leading and trailing edge signal receives a high-precision time stamp, which is retained, together with the corresponding channel number, in a large internal buffer of the TDC ("Level-1 buffer").

When the TDC receives a Level-1 trigger, a subset of the recorded hits, corresponding to a pre-defined time window, are retained for readout and are forwarded to the data concentrator of this chamber, the "Chamber Service Module" (CSM). From there, data are sent to the off-chamber electronics in USA15, the "Readout Driver" (ROD). A CSM can serve up to 18 mezzanine cards. The operation parameters of the analog frontend (ASD) and the TDC are controlled by a JTAG string, which is distributed by the Detector Control System (DCS) to the CSM, which sends it individually to each mezzanine card. Fig. 3 gives the layout of the present system. A detailed presentation of the MDT readout electronics is given in [4]. The ASD and TDC ASICs are described in [6] and [7].

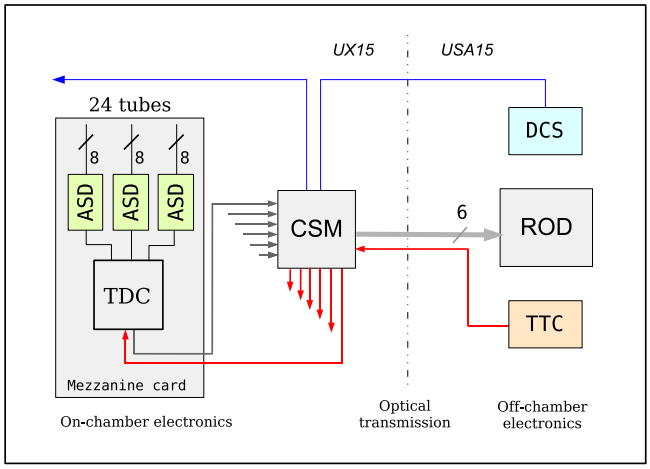


Figure 3: Schematic diagram of the present MDT readout chain. The Chamber Service Module (CSM) collects all data of a given chamber and sends them to the ROD via an optical link. Up to 18 TDCs, corresponding to 432 tubes, can be serviced by a CSM. The 40 MHz clock and the Level-1 trigger are broadcast by the TTC system to the TDCs.

### 5.5.2 Architecture of the readout for MDTs with Small tubes

For the evolution of this architecture into matching the requirements of the Small tube readout, a number of problems limiting the performance of the present scheme has to be overcome. Given the high rate capability of the Small MDT tubes, the bandwidth of the readout system has to be increased. Due to the limitations of the internal buffering scheme and processing speed, the present TDC can only handle average tube rates up to about 300 kHz per tube without losing data, while Small tubes would operate beyond 1 MHz per tube. Therefore, an improved TDC is an essential requirement for a new readout design. Another limitation of the readout

bandwidth comes from the optical link, connecting the CSM to the ROD, as the S-link protocol only supports a usable bandwidth of 1,4 Gbit/s. Fig. 5 shows occupancy and efficiency of Large and Small tubes as a function of tube hit rate.

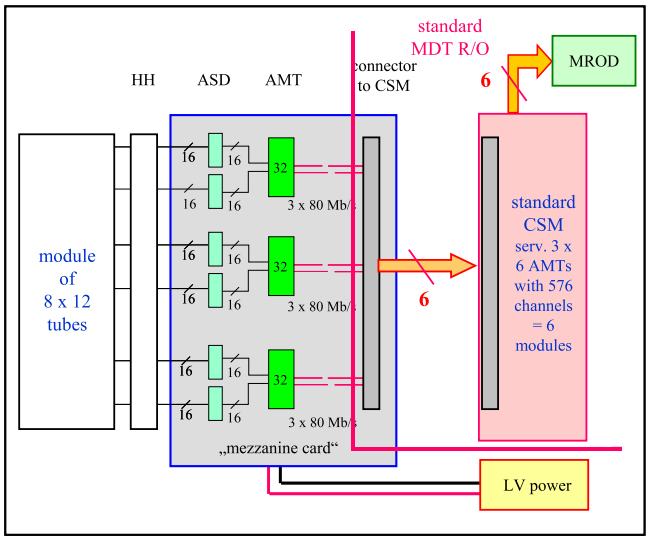


Figure 4: Schematic diagram of the chain for the readout of the Small tube chambers. The higher tube density at the tube ends requires a higher modularity for the readout architecture.

When upgrading the performance of ASICs (ASD, TDC), we have to take into account that their technologies are no longer supported by industry. The following new components had therefore to be introduced into the readout system.

- The ASD is re-designed in the IBM 130 nm technology. A 4-channel prototype, demonstrating the analog parameters, has already been produced and works correctly. Most analog parameters of the previous design are preserved.
- The TDC will be replaced by the HPTDC, designed by the CERN-MIC group ( [5]). This 32-channel device has an improved internal buffering scheme as well as higher transfer and processing speeds.
- The CSM collects data from a MDT chamber formats the event and sends data, trigger-by-trigger, via an optical link to the ROD in USA15. All logical operations are performed by an FPGA, which will need to be upgraded to higher radiation tolerance. The interface to DCS, needed for controlling electrical and temperature parameters on the chamber will be done via the GBT (see below). The adapter box to the CANbus (ELMB) can therefore be dropped, reducing complexity of cabling.
- The link connecting the CSM to the ROD will be replaced by a GigaBit Transmitter link (GBT), developed by CERN. This link provides a 3 times higher transfer rate (Gbit/s), compared to the S-link [8].

Another stringent requirement for the practical realization of the new readout scheme is the mechanical integration of the on-chamber readout electronics with the chamber mechanics, as the density of channels at the tube ends is four times higher than in the case of the Large tubes. The following design changes will therefore be implemented.

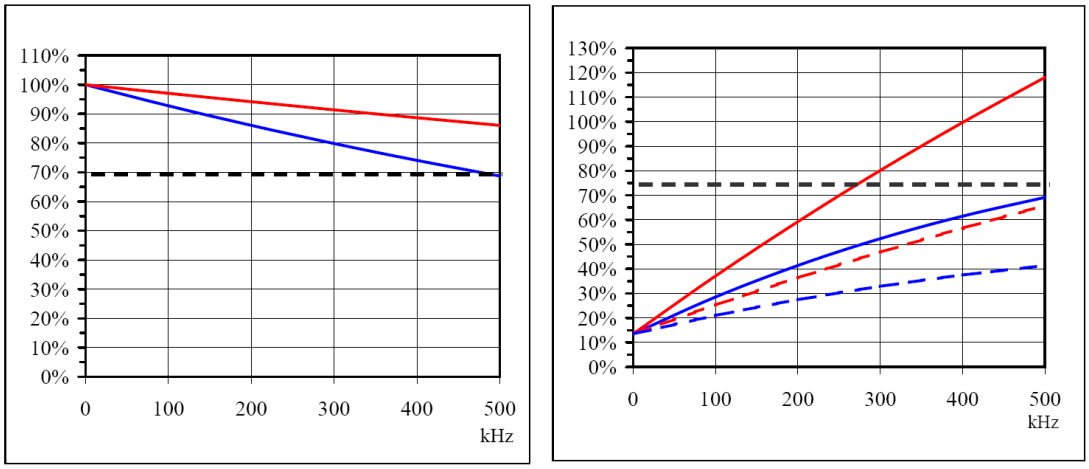


Figure 5: Efficiency (left) and saturation of the readout link between TDC and CSM in edge mode (right) as a function of the tube hit rate for dead time 750 ns (blue) and 200 ns (red). The dotted curves in the right diagram correspond to pair mode. The dotted horizontal line marks the minimum efficiency required for reliable tracking (left) and the maximum saturation level recommended for the readout. **This numbers will be checked. Why is this curve non-linear? The diagrams will be simplified.**

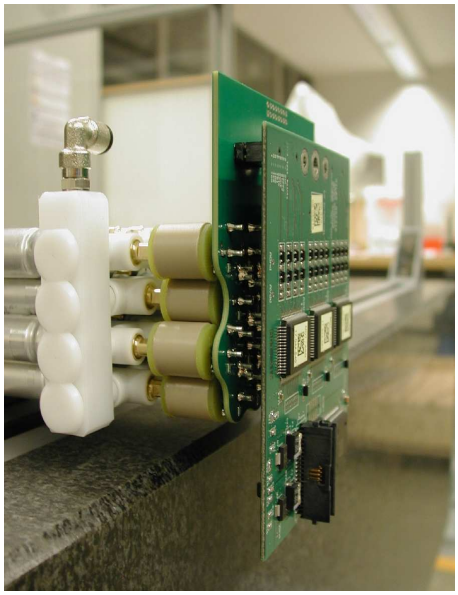

Figure 6: Space requirements at the tube ends on the Small tube chambers necessitate a separation of the HV-coupling capacitors from the signal routing card ("hedgehog card"). The HV capacitor is mounted in a small Noryl (??) cylinder.

- HV decoupling capacitors are located in 15 mm diameter cylinders at the tube ends, see Fig. B.1and Fig. 6. The density of signal routing on hedgehog cards is thus no longer limited by HV insulation distances between HV and signal traces on the PCB.
- To match the higher tube density, the space on the mezzanine card has to be used more efficiently. For this purpose, the passive protection circuitry of the ASD inputs will be moved to the hedgehog card. In addition, the modularity of the ADSs will be changed from 8 to 16 channels per chip, which goes well with the 32-channel modularity of the

HPTDC.

- For the interconnection between mezzanine cards and New CSM we foresee to use the same 40-wire cables as was used in the present system. Its moderate diameter and high flexibility may be important for fitting the new MDTs into the limited space in the Small Wheel.
- While the power dissipation of the on-chamber frontend electronics of the present system was xx W/channel, leading to a dissipation of yy W/m in multilayers with 4 tube layers, the dissipation would now be about zz W/m. This may require flushing with dry air or even liquid cooling, as natural air convection is hampered by the tight space constraints of the Small Wheel.

Now something about mechanics, real estate, component density, packaging etc.

Finally something about rates.

### 5.6 Services, infrastructure, and DCS !!! RR+JD to supply text !!!

1. *Description of service scheme (including power system, read-out, trigger, alignment), cooling needs and other special requirements*
2. *Table with number of services (number of cables, outer diameter, cross section of leads)*
3. *Table with power consumption (per channel, chamber, total)*
4. *Required rack space*
   (a) *UX15 (include maximum allowed distance to detector if any)*
   (b) *US15 (power system)*
   (c) *USA15 (DAQ)*
5. *Gas system and distribution*
   *Details on number of gas manifolds per sector (include drawings) and connections to chambers (serial, parallel?)). Size of pipes*
   *Required nominal, minimum, and maximum flow*
   *Required precision of gas mixture*
   *Safety measures in case of inflammable gas*
   *Required rack space for gas system in SGX1, USA15, UX15*
6. *Integration in DCS system, requirements for DCS !!! Via GBT or ELMB++ ?? !!!*

## 6 Expected muon performance with NSW [SV]

*Discussion of overall performance. L1 trigger, muon reconstruction, efficiency, fake, sensitivity to a few layout parameters (number of layers, ...),*

| Cable | Number of cables (granularity) | Outer cable diam. (mm) | Cross section of leads ($mm^2$)) |
|---|---|---|---|
| HV | | | |
| LV | | | |
| Monitoring and control | | | |
| Front-end links | | | |
| Calibration | | | |
| Alignment | | | |
| Miscellaneous | | | |

Table 2: Example table number of services per chamber

| Chamber | Number of channels | Power consumption per channel | Total power consumption |
|---|---|---|---|
| | | | |

Table 3: Example table: Number and types of chambers per sector

# 7 Integration, assembly and commmissioning [JD]

# 8 Cost, resources and schedule [LP, TK]

# 9 Conclusions

# Appendices

# A Radiation background

*Discussion of expected cavern background and its uncertainty based on simulations and measurements with muon detectors, and finally give a reference figures and safety factor.*

- *Overview of cavern background. It's nature, origin, shielding strategy*
- *Simulation result. R distribution in the small wheel region. 14 TeV, Al beam pipe, 14 TeV steel beam pipe, 7 TeV steel beam pipe.*
- *Measuremenents with pp collision. MDT, CSC*
- *Summary figure. Reference figures.*

## A.1 simulation

# B Small tube

*Detail of detector technologies proposed for use in the small wheel detector, including the status of developments. Include a description on the status and size of available prototype chambers.*

*This section should describe the technology up to the level of a single chamber.*

## B.1 Tracking in a high–background environment

The reduction of the tube diameter of the MDT tubes allows to maintain the main advantages of the drift tube concept:

(a) independence of the position resolution from the angle of incidence onto the chamber plane (contrary to drift chambers with rectangular drift geometry)

(b) operational independance of each tube, where any malfunction of a tube can only generate a negligible inefficiency

(c) modularity of chamber construction.

To verify the performance of 15 mm ("small") tubes a number of tests was executed, using cosmic muon tracks. A pair of 30 mm ("large") drift tube chambers was used as reference, defining the position of the muon track, while a layer of small tubes was the device under test.

Tubes along the track are called 'efficient' when the hit is detected inside a $3\sigma$ road, as defined by the reference tubes.

This measurement was done in the presence of adjustable levels of gamma background due to the GIF facility at CERN [10]. Fig. 2 shows the efficiency of small and large tubes vs. hit rate from gamma conversions. As expected, small tubes provide a much better performance at high background rates. The efficiency at rate zero deviates from 100 % due to tracks passing across or close to the tube walls and due to $\delta$-electrons shifting the hit position outside the $3\sigma$ acceptance road. The average position resolution in the small tubes was about 120 $\mu$m. Due to the short drift compared to large tubes, this value showed little dependence on the background rate.

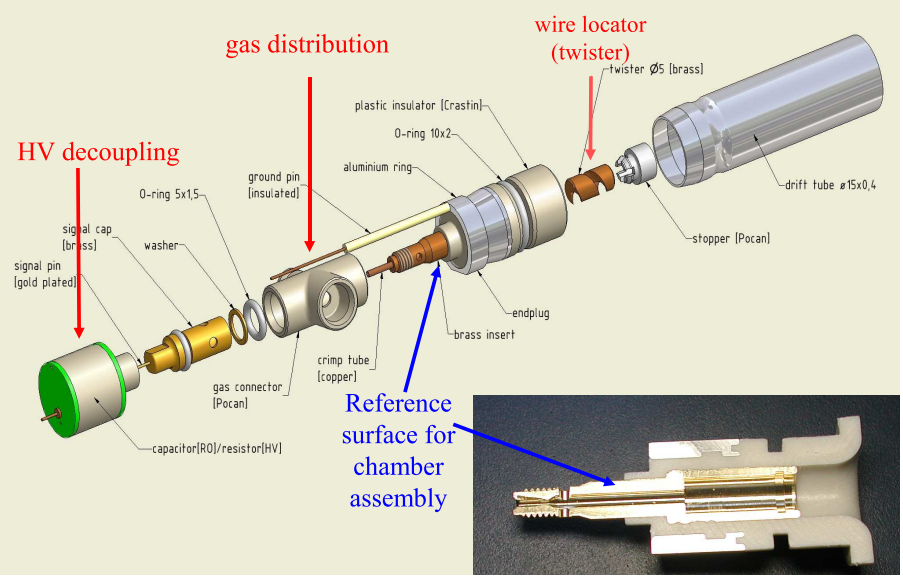


Figure 1: Structure of a small drift tube with gas connection and decoupling capacitor in the longitudinal direction (green cylinder). The plastic parts are injection moulded.

## B.2 Technical Implementation

Going from large to small tubes as construction elements for MDT chambers poses a number of technical challenges, as the higher tube density requires more refined electrical and gas connections on the same available service area.

Hier comes figure 6 (not displayed because of big size).

A particular problem is the supply of the tubes with the operating voltage of 2730 V, requiring isolation distances which cannot be realized on the area available for the readout boards. The integration of the HV decoupling capacitors into the end-plugs of the tubes was therefore a central requirement for the tubes. In a similar way, gas supplies had to be simplified to facilitate the integration of the tubes. Fig. B.1 shows the tube design, HV capacitor and gas distribution being integrated into the structure of the end-plug.

The integration of tubes into chambers is achieved by bonding tubes layer by layer with

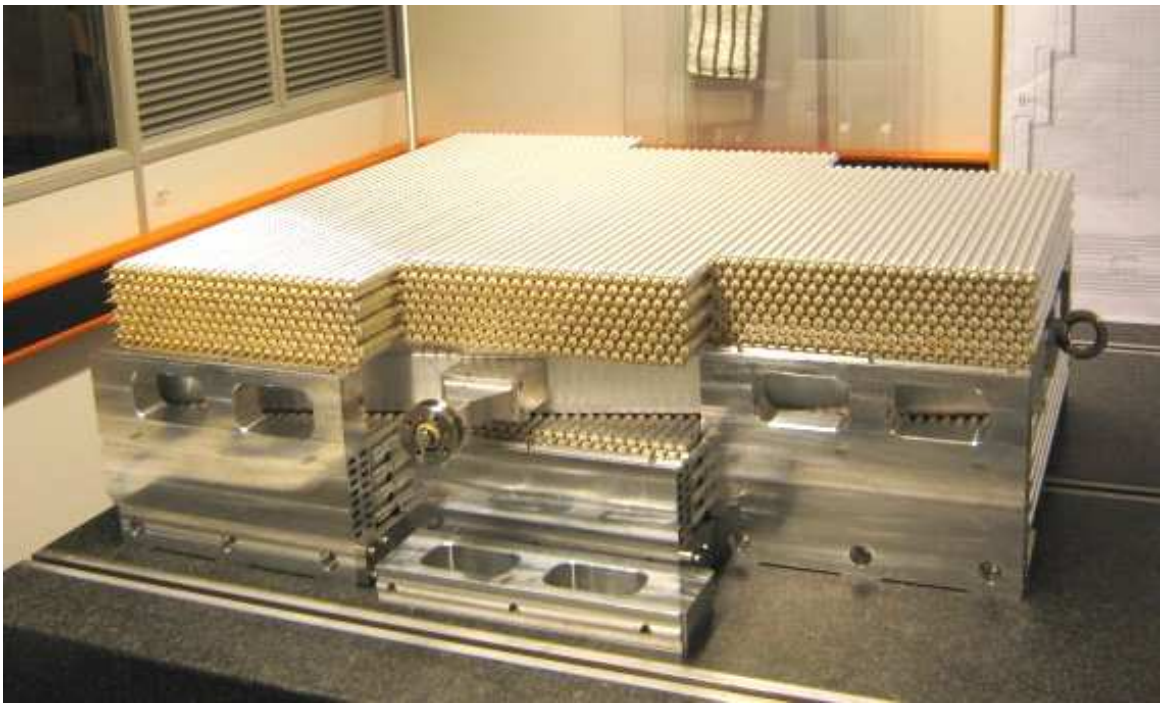

Figure 2: The small tube prototype chamber after assembly, consisting of two modules of 8 tube layers, 72 tubes per layer and 1152 tubes in total.

epoxy glue. In production tests, tubes were fixed in precision supports ("combs") during curing, and the target accuracy of 20 $\mu$m was obtained. A module with 8 tube layers was glued in a time span of a few hours. With curing overnight, the assembly of a module took only one day.

Presently, a full prototype of a MDT chamber in small tube technology is under construction. It consists of 2×8 tube layers and is designed to fit into the inner part of the muon detector in the very forward direction, where rates are highest (Fig. B.2). This prototype will be available for tests in a muon beam at CERN and in the GIF facility in summer 2010. The readout will be achieved with available electronics for the large tube chambers, specially adapted for use with the new chamber geometry.

## B.3 Assembly

*Describe the assembly procedure. Include details on*

1. *Achieved mechanical precision of signal generating parts (i.e. strips or wires)*
2. *Speed of assembly*
3. *Splitting of work and logistics between production site*

## B.4 Quality Assurance and Commissioning

1. *Quality assurance of all individual chamber parts, include necessary manpower and rate of tests*
2. *Quality assurance and commissioning scheme of full chambers, include necessary manpower and rate of tests*
3. *How can/is data of the commissioning used later (e.g. strip or wire positions)?*

*Note: A common commissioning strategy during and after assembly of the wheels will be given in a previous chapter*

## B.5 Operation, Maintenance and Safety

*Describe in detail the impact of failures of single components (gas leak, HV breakdown, front-end electronics) on the detector operation. Comment on possible built-in redundancy.*

*Describe in detail the possible scenarios for maintenance on the detector and the exchange or repair of detector parts.*

*Describe the risks associated with the technology during operation and maintenance (HV, maximum currents, flammable gas etc.)*

## B.6 Performance

*Describe in detail the performance of the detector, including results from test beam studies. Include studies with background radiation ($\gamma$, n, p)*

1. *Detector occupancy as function of rate*
2. *Spatial and angular resolution as functions of rate and angle of incidence for single point measurements and segments*
3. *Time resolution*
4. *Efficiency (single measurement and segment)*
5. *Double track resolution*
6. *Rejection of fake and background tracks*
7. *Sensitivity to background radiation*
8. *Performance limits (maximum rate)*

## B.7 Aging Tests

*Describe in detail results from aging tests for all components, the detector itself including the on-chamber gas distribution, read-out and/or trigger, alignment, and detector control electronics.*

## B.8 Cost, Funding, and Manpower

1. *Table of cost of each component, full chambers and total*
2. *Additional costs (e.g. integrating two technologies)*
3. *Arrangements for funding (if any so far)*
4. *List of manpower needs, especially include statements on the the current and future availability of experts (for at least the full construction and commissioning period, i.e. 2012 – 2019, better also for the operation)*

# C TGC

# D RPC

# E Micromegas

# References


[1] G. Aad et al. Expected Performance of the ATLAS Experiment - Detector, Trigger and Physics. 2009.

[2] G. Aad et al. The ATLAS Experiment at the CERN Large Hadron Collider. *JINST*, **3** S08003 (2008)

[3] M. Bosman et al. Estimation of Radiation Background, Impact on Detectors, Activation and Shielding Optimization in ATLAS, ATLAS Note *ATL-GEN-2005-001* (2005)

[4] Y. Arai et al., ATLAS Muon Drift Tube Electronics, *JINST* **3** P09001 (2008)

[5] J. Christiansen et al., Manual and User Application Notes for the HPTDC, (2004), *http:/tdc.web.cern.ch/tdc/hptdc/docs/hptdc_manual_vs2.2.pdf* and *http:/tdc.web.cern.ch/tdc/hptdc/hptdc.htm*

[6] Posch C., Hazen E., Oliver J., MDT-ASD User's Manual, (2007), ATL-MUON-2002-003; *https://edms.cern.ch/document/899037/2/ASD_Manual_vs_2007.pdf*

[7] Y. Arai, AMT-3 User Manual, *https://edms.cern.ch/file/897562/1/AMT3manual_033.pdf, http://atlas.kek.jp/tdc/amt3/AMT3manual_033.pdf*

[8] P. Moreira, find some reference to the GBT!!

[9] M. Deile et al., *Performance of the ATLAS Precision Muon Chambers under LHC Operating Conditions*, Proceedings of the $9^{th}$ Pisa Meeting on Advanced Detectors, Isola d'Elba, Italy, 25–31 May 2003, Nucl. Instr. and Methods **A518** (2004) 65;
M. Deile et al., *Resolution and Efficiency of the ATLAS Muon Drift-Tube Chambers at High Background Rates*, Proceedings of the $10^{th}$ Vienna Conference on Instrumentation, Vienna, Austria, 16–21 February 2004, Nucl. Instr. and Methods **A535** (2004) 212;
S. Horvat et al., *Operation of the ATLAS Muon Drift-Tube Chambers at High Background Rates and in Magnetic Fields*, IEEE Transactions on Nuclear Science, Vol. 53, No. 2 (2006) 562.

[10] J. Dubbert et al., *Development of Precision Drift Tube Detectors for the Very High Background Rates at the Super-LHC*, Proceedings of the 2007 IEEE Nuclear Science Symposium, Honolulu, Hawaii, USA, 28 October–2 November 2007; MPI report, MPP-2007-172, November 2007.